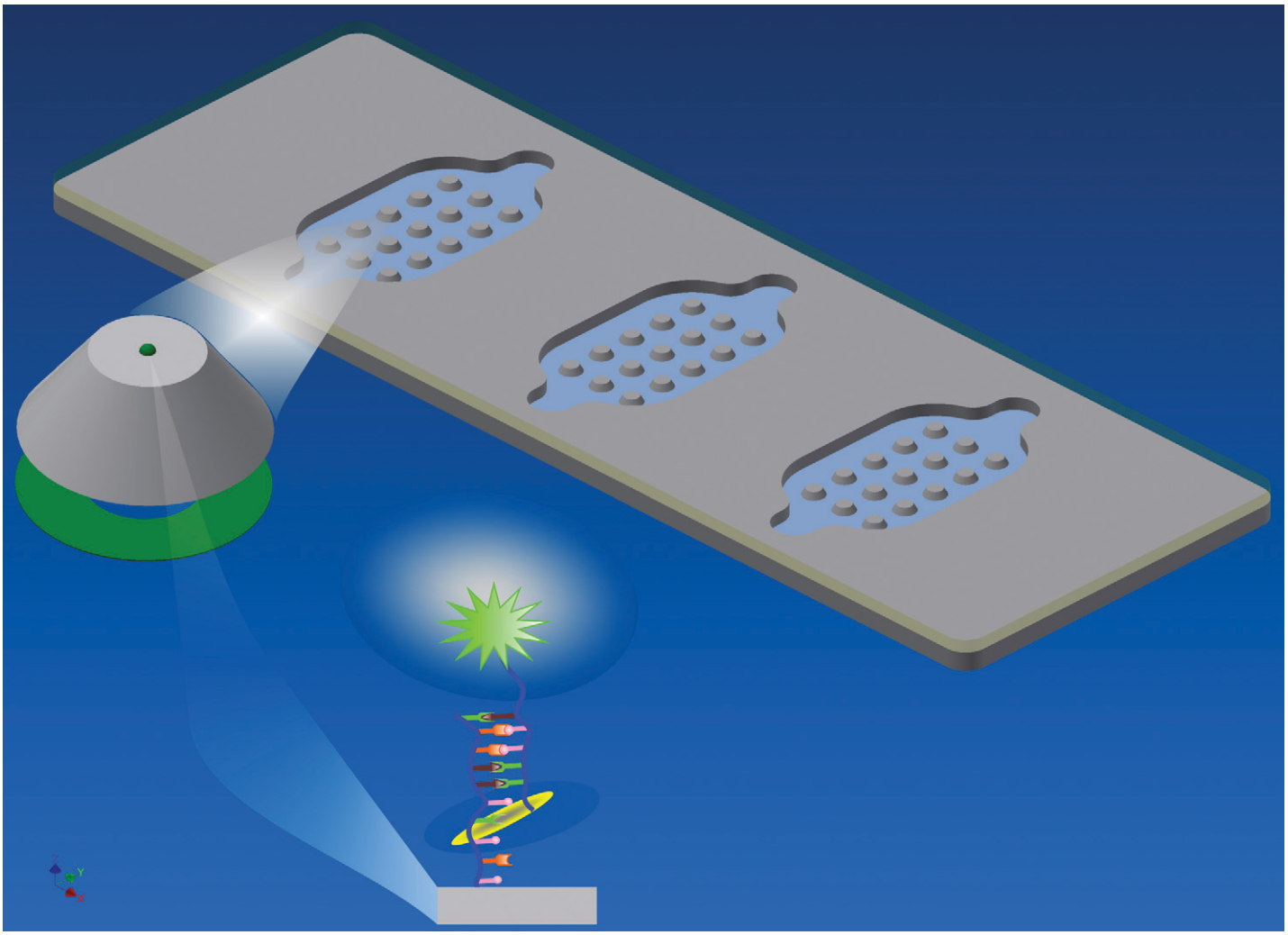

Showcasing research from the BIOLABCHIP group of Prof. Anders Wolff, Technical University of Denmark, DTU Bioengineering

Optimising the supercritical angle fluorescence structures in polymer microfluidic biochips for highly sensitive pathogen detection: a case study on *Escherichia coli*

Supercritical angle fluorescence structures allow the observance of surface fluorescence at about 46-folds higher intensity than with a conventional microscope. This paper demonstrates a method for the optimisation and massive production of supercritical angle fluorescence micro-array structures on-chip for use with multiplex solid-phase PCR for the detection of pathogens.

As featured in:

See Trieu Nguyen, Anders Wolff *et al.*, *Lab Chip*, 2019, **19**, 3825.

ROYAL SOCIETY OF CHEMISTRY | Celebrating IYPT 2019

rsc.li/loc

Registered charity number: 207890

Lab on a Chip

PAPER

View Article Online
View Journal | View Issue

Cite this: *Lab Chip*, 2019, **19**, 3825

Optimising the supercritical angle fluorescence structures in polymer microfluidic biochips for highly sensitive pathogen detection: a case study on *Escherichia coli*†

Trieu Nguyen, ‡[a] Tien Anh Ngo, ‡§[b] Dang Duong Bang [b] and Anders Wolff*[a]

In this paper, we present, to the best of our knowledge, for the first time, in-depth theoretical analysis and experimental results for the optimisation of supercritical angle fluorescence (SAF) structures in polymer microfluidic chips fabricated from a combination of micro-milling and polymer injection-moulding techniques for their application in the highly-sensitive detection of pathogens. In particular, we address experimentally and theoretically the relationship between the supercritical angle and the heights of the SAF structures embedded in the microfluidic chips to obtain optimised results where the highest fluorescence intensity is collected, and hence determining the optimised limit of detection (LOD). Together with theoretical modelling, we experimentally fabricate microarrays of SAF structures with different heights varying from zero to the order of 300 μm in cyclic olefin copolymer (COC) microfluidic chips. The results show that for fluorophores at the interface of air and COC, the highest fluorescence intensities are obtained at SAF structures with a 163 μm height for a milling tool with a 97.4 μm diameter, which is in excellent agreement with our modelling. A fluorescence LOD of 5.42×10^4 molecules is achieved when using such SAF structures. The solid-phase polymerase chain reaction (SP-PCR) on these SAF structures permits sensitive pathogen detection (3.37×10^2 copies of the *E. coli* genome per μL) on-chip. These results especially are of interest for applications in hypersensitive pathogen detection as well as in assisting the design of devices for point-of-care applications. Findings on the height optimization of SAF structures also advance our understanding of SAF detection techniques and provide insights into the development of fluorescence microscopy.

Received 6th September 2019,
Accepted 5th October 2019

DOI: 10.1039/c9lc00888h

rsc.li/loc

1. Introduction

Excited fluorescent molecules positioned at a distance less than their emission wavelength to the interface of two dielectric media emit a large amount of their radiation into the higher refractive index medium[1–9] (Fig. 1). The angle at which significant emission can be observed in the denser medium is called the supercritical angle since it is above the angle of total internal reflection, *i.e.* the critical angle of the two media. The fluorescence observed in this context is hence called supercritical angle fluorescence (SAF).

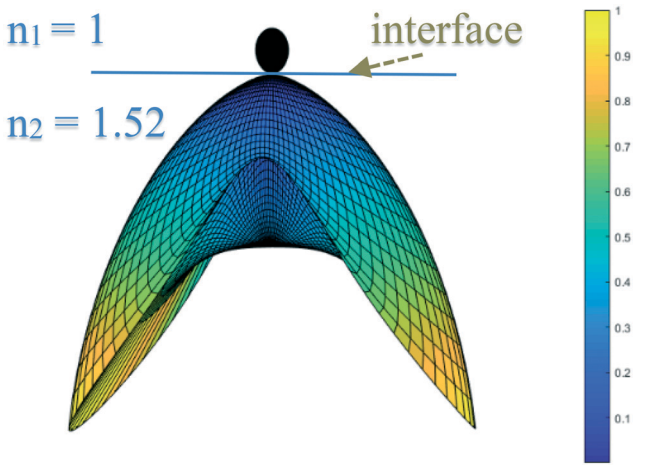

Fig. 1 Radiation pattern of an electric dipole (fluorophore) positioned in the vicinity of the interface between two media with reflective indices n_1 and n_2 in which n_2/n_1 = 1.52. A large portion of radiating emission is observed in the denser medium at an angle above the critical angle. The figure is adapted from the studies in ref. 1 and 8.

[a] *Department of Biotechnology and Biomedicine, Technical University of Denmark, DK-2800 Kgs. Lyngby, Denmark. E-mail: awol@dtu.dk*
[b] *Laboratory of Applied Micro and Nanotechnology (LAMINATE), Division of Microbiology and Production, National Food Institute, Technical University of Denmark, Kemitorvet, Building 204, DK 2800 Lyngby, Denmark*

† Electronic supplementary information (ESI) available. See DOI: 10.1039/c9lc00888h

‡ T. Nguyen and T. A. Ngo contributed equally.

§ Current address: Vinmec Biobank, Vinmec HealthCare System, 458 Minhkhai, Hanoi, Vietnam.

Recently, the fluorescence from Cy5-labelled antibodies collected efficiently at the surface of a solid paraboloid element using the SAF phenomenon has been applied to measure the inflammatory marker C-reactive protein (CRP) in the clinical range in serum.[10] Ruckstuhl *et al.* reported another platform using SAF immunoassay to detect analytes. The optics for the screening of SAF was built into a disposable polymer tube which offered the highly sensitive readout of solid-phase immunoassays in real-time.[11] The solid elements used to observe SAF from the interface due to total internal reflection are called SAF structures. These SAF structures are in the millimetre range in the studies in ref. 10 and 11. The development of micro- and nano-technology in the last two decades leads to opportunities for the fabrication of structures and devices, which can be employed in the rapid and highly sensitive detection of reagents with low concentrations and volumes. Instead of using millimetre-range solid paraboloid elements, our group has developed a technique to fabricate micro cone-shaped SAF arrays on which multiplexed detection of pathogens with high sensitivity and a low volume of reagents were achieved.[8,12] The detection technique is carried out based on two portions: (i) using solid-phase PCR and (ii) fabrication of micro SAF arrays. In the fabrication step of micro SAF arrays, the size optimisation of the SAF structures, however, has not yet been conducted, which gives rise to limitations of and obstacles in this method in massive chip production for industrial applications, *e.g.* in point-of-care detection devices. There must be a relationship between the critical angle and the height of the SAF structure (which in turn will define the SAF structure size) so that the maximum fluorescence intensity can be observed, and hence the optimised limit of detection (LOD) can be determined. From the optimised height, if the SAF structures are too high, the fluorescence observation can be disturbed by optical noise due to the increase of the surface area and hence the surface roughness at the sidewalls.[8] When the height of the SAF structure is too low, we lose the observation signal due to reaching the limit of the supercritical angle and total internal reflection.[1]

In this work, we present, for the first time, both experimental and theoretical investigation on the optimisation of fabricating SAF microarrays used in hypersensitive pathogen detection. We first show theoretical modelling to obtain the optimal height of the SAF structures. To verify this theory, experiments on the design and fabrication of SAF structures with different heights are then carried out. The resulting SAF structures with different heights are characterized with SEM and a Dektak and a non-contacting (optical) surface profiler. The polymer chips containing these SAF structures are then verified using a fluorescence nano-spotting machine and scanner to observe the highest fluorescence intensity, which corresponds to the optimal height of the SAF structures. Afterwards, the optimal chips are used to detect *Escherichia coli* (*E. coli*) and to obtain the LOD experimentally.

2. Theoretical modelling and experimental fabrication

Fabrication of polymer chips is carried out with polymer injection moulding using a Victory 80/45 Tech injection moulding system (Germany). Cyclic olefin copolymer (COC), grade 5013L-10 (TOPAS Advanced Polymers GmbH, Frankfurt-Höchst, Germany), is used in the experiments.

2.1. Modelling of the optimal height of the SAF structures

The insert (shim) for injection moulding is made by (micro) milling a hard aluminum plate (Alloy 2017, MetalCentret, Denmark). In order to obtain cone-shaped microarrays, the milling tip of the engraving tool must also possess a cone shape, as shown in Fig. 2a.

Fig. 2c shows the schematic of a SAF structure. Fig. 2b shows the SEM image of a typical SAF structure (taken from one of our chips) made by polymer injection moulding using an insert fabricated with a micro-milling machine employing a 60° engraving tip.

As aforementioned, a fluorescent molecule located at the interface of the two media with different refractive indices emits a large portion of angular radiation into the denser medium. The SAF structures in this work hence serve two

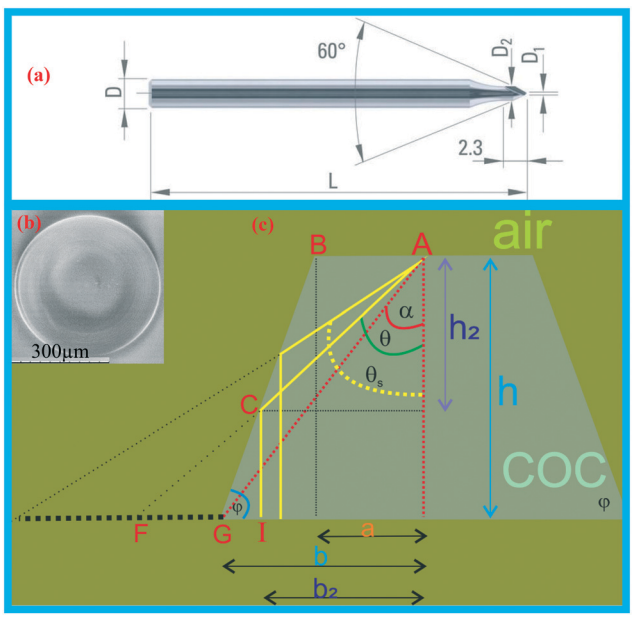

Fig. 2 (a) Schematic of a 60° engraving tip (DIXI 7006, Le Locle, Switzerland), picture from the company website in ref. 13. (b) SEM image of a typical SAF structure fabricated in our experiments. (c) Schematic of the SAF structure obtained using a micro-milling shim and polymer injection moulding; in this schematic, a fluorescent molecule is located at point A and its emitted light is represented by the yellow lines. The olive coloured area represents the medium with refractive index n_1 (air), and the grey colour represents the polymer with refractive index n_2 (COC). θ is the critical angle of the two media. θ_s ($>\theta$) is the supercritical angle of the two media. α is the geometry angle. φ is the angle of the milling tip, φ = 60°.

purposes: (i) to be a high refractive index medium and (ii) especially the cone-shaped structures, act as mirrors in terms of total internal reflection to collect the emission light effectively at an angle above the critical angle.

According to the law of refraction (Snell's law), the critical angle for the two media in our investigation (air, n_1 = 1, and COC, n_2 = 1.53) is $\theta = \arcsin\left(\frac{n_1}{n_2}\right) = 40.8°$,[12] see Fig. S2 in the ESI† for the measurement of COC refractive index. The supercritical angle at which a large portion of angular radiation is emitted should be greater than or equal to (≥) the critical angle (θ),[10] denoted as θ_s in Table 1, see also Fig. 2c. Here, in this paper, we for the first time demonstrate that for SAF structures fabricated by polymer injection molding using a micro-milling insert (as shown in the schematic in Fig. 2c), the optimal height is achieved when the lower limit (or the minimum) of the supercritical angle θ_s (*i.e.* θ_{s_min} = the critical angle θ) is equal to the geometry angle (α). Further, from that, we originally derive the formula for determining the optimal height of SAF structures fabricated by a micro-milling method and polymer injection moulding.

Here, we show the summary for the theory and details are shown in the ESI.† Due to the symmetric geometry of the SAF structure, without losing the generality, we consider the model for only one-half of the SAF structure. From Fig. 2c, we can see that the emission light (represented by the yellow line **AC**) undergoes total internal reflection, which is then represented by line **CI** and at point **I**, one can observe the fluorescence intensity. It can be seen that in the dead (useless) area, denoted as triangle **CGI**, there is no fluorescence to be observed. Line **GI** hence takes up space but is useless, and it makes the SAF structures bigger and especially taller. As a result, a bigger reaction-chamber would be needed to be fabricated.

Moreover, with larger SAF structures, a lesser number of them can be made for the same volume of one reaction chamber, and that could limit the opportunities to conduct multiplex detection. Furthermore, as for the polymerase chain reaction technique, the lower the reaction chamber volume (hence the lower thermal mass), the more convenient is the design and the better is the heating and cooling performance of the thermal cycler.[14,15] Besides, portability is also one of the requirements for point-of-care devices.[16,17] The optimisation of the SAF structure height is hence essential.

The optimal size of the SAF structures can hence be obtained if the area of triangle **CGI** approaches zero. This means that the length of line **GI** = 0, *i.e.* line **GI** (or the two points **G** and **I**) in Fig. 2c move to and take up the position of point **C**. Mathematical calculations (details are shown in the ESI†) result in **GI** = 0 when $\theta = \alpha$. Consequently, the derivation for the optimal height of the SAF structures is expressed as:

$$h = \frac{a\tan(\phi)}{\tan(\theta)\tan(\phi) - 1} \quad (1)$$

Table 1 Notations used in this section

Notation	Functions
a	Half of the diameter of the top circle of a SAF structure
b	Half of the diameter of the bottom circle of a SAF structure
c	$= b - a$
h	Height of a SAF structure
θ_s	Supercritical angle
φ	SAF angle (the angle created from the milling tip), in this case, equals to $\pi/3$ radians
α	Geometry angle
D_1	$= 2a$, the diameter of the top circle of a SAF structure
n_1	= 1, the refractive index of air
n_2	= 1.53, the refractive index of COC

2.2. Chip fabrication

For fluorescence intensity measurements at the optimised height of the SAF structures, the experiments and chip fabrication are done in two batches. In the first batch, we fabricate an 8-chamber microfluidic chip on which each chamber has eight different heights of SAF structures varying from 0, 10, 20, 50, 100, 150, 200, and 300 microns. We have also fabricated a cyclic olefin copolymer (COC) microfluidic chip with 8 chambers for batch number two, and each chamber has a SAF microarray with different heights varying from 0, 10, 20, 50, 100, 150, 200, and 300 microns, respectively (Fig. S3 and S4†).

3. Experiments on the fabricated chips

3.1. Experiments to determine the fluorescence intensity on the SAF microarrays

The optimal height of the SAF structures, where the highest fluorescence intensity was observed, was confirmed by spotting a solution containing Cy3-labelled oligonucleotide 10T10C (5′-Cy3-TTTTTTTTTTCCCCCCCCCC) in 5× standard saline citrate (SSC) and 0.004% Triton X on the top of each SAF structure. The precise spotting volume on the top of each SAF structure was determined using a sciLEXARRAYER S5 (Scienion, Germany). The intensities of Cy3 fluorescence on each SAF structure were analysed using a BioAnalyzer 4F/4S scanner (LaVision Biotec GmbH, Bielefeld, Germany).

Fluorescence intensities were determined using ImageJ 2.1. A circle was sized to the size of the SAF structure, and the mean value of grey levels of the pixels inside a fluorescent spot was then computed. To determine the signal to noise ratio (SNR), the mean signal fluorescent spot with the sample without a probe target (negative control, NC) was used as a background. The SNR in this study was defined as the mean signal intensity of the feature subtracted by the mean background and divided by the variation of the background. The limit of detection (LOD) was determined at a SNR of 3.[18] All the experiments were performed in triplicate.

Table 2 List of primers used in this study

Primers	Sequences
Forward primer	5′-GTGTGATATCTACCCGCTTCGC-3′
Cy3-labeled reverse primer	5′-Cy3-AGAACGGTTTGTGGTTAATCAGGA-3′
Surface primer	5′-TTTTTTTTTTCCCCCCCCCCTCGGCATCCGGTCAGTGGCAGT-3′

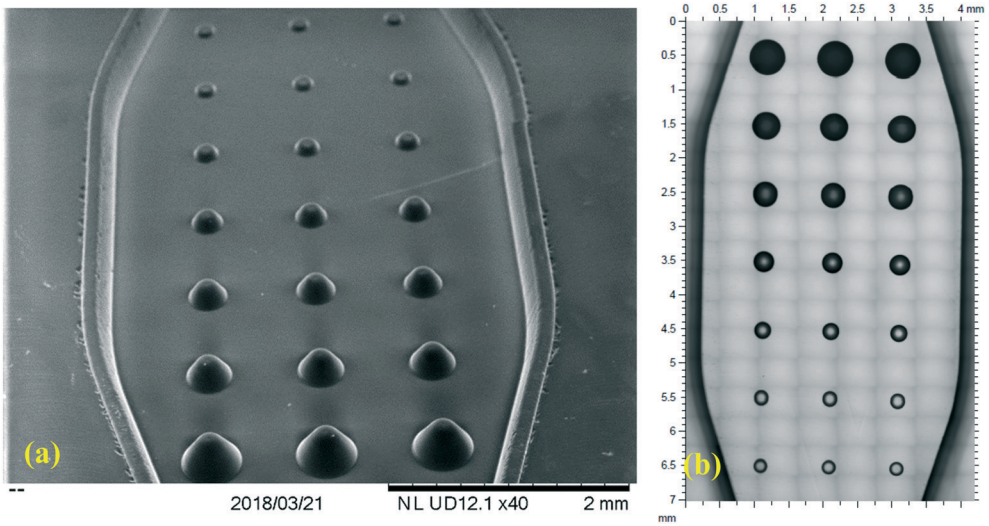

Fig. 3 (a) SEM image (side views) of the SAF structures with different heights inside the reaction chamber of the polymer chip. (b) Top view of the same chamber using a PLu Neox 3D optical profiler (from Sensofar). The optical profiler is a non-contact profiler, and this picture is captured using the stitching function of the Sensofar optical profiler so that an overview of the whole chamber can be shown. The uniformity of the fabricated SAF structures can be seen both with SEM (a) and the Sensofar optical profiler (b).

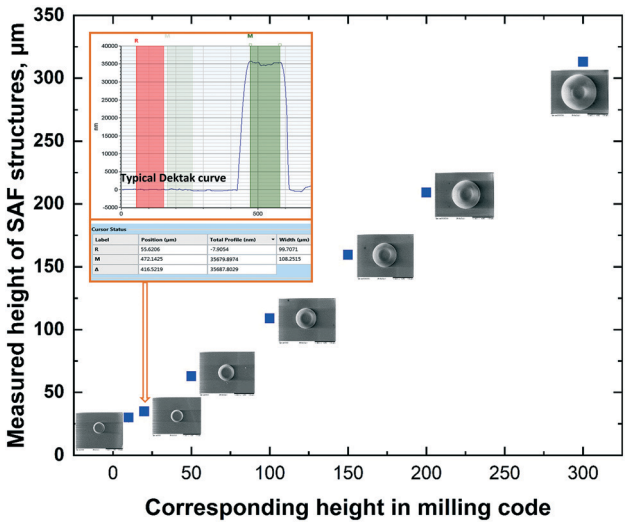

Fig. 4 Blue data points represent the heights of the fabricated SAF structures in the polymer chip measured using a Dektak XTA stylus profiler. Inset shows the typical Dektak curve (the other Dektak curves for the other SAF structures have the same form, hence in this figure we show only one typical Dektak curve). The height value from this typical Dektak curve of the inset figure is shown as the second data point (see the orange arrow pointing to it, ~35 µm in the vertical axis). Near to each data point, the SEM images of the top view of the SAF structures are shown.

3.2. Solid-phase PCR on SAF microarrays in a microfluidic chip for bacterial pathogen detection

3.2.1. Sample preparation. *Escherichia coli* (CCUG 17620) (*E. coli*) originating from the Culture Collection of the

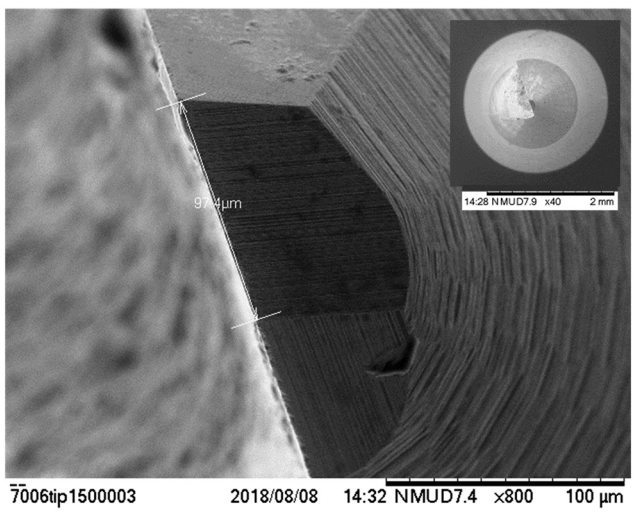

Fig. 5 SEM image of the milling tip (engraving tool 3/4); the diameter of the tip is measured and is equal to 97.4 µm. Inset is the zoom-out (low magnification) SEM image of the entire milling tip. The diameter of the milling tip is important since it determines the size of the SAF structures.

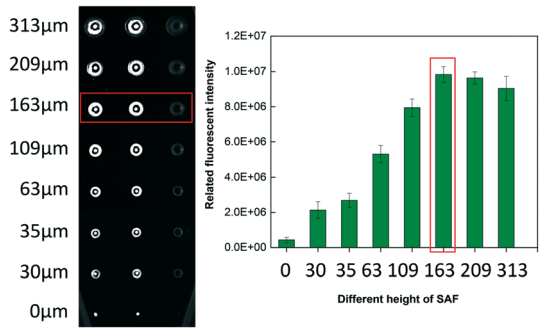

Fig. 6 (Left) The fluorescence image of the SAF structures after scanning. (Right) The fluorescence intensities *versus* different SAF heights in the same reaction chamber.

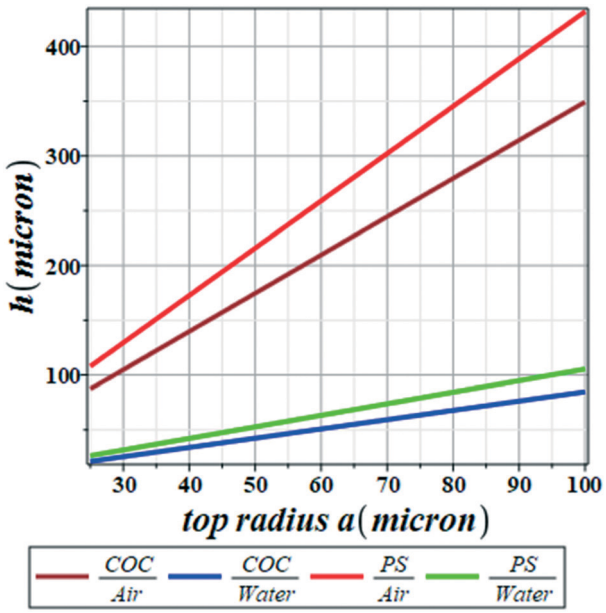

Fig. 7 Theoretical prediction of the optimal SAF heights for different materials (COC and PS), different working conditions (water and air) and different milling tips (parameter *a*).

University of Gothenburg (Sweden) was from a bacterial strain collection of the National Food Institute, Technical University of Denmark (DTU-Food). *E. coli* genomic DNA was isolated using a DNeasy Blood and Tissue kit (Qiagen, Germany) according to the instructions from the supplier. The DNA concentration was determined using a Nanodrop (Thermo Scientific, USA) and stored at −20 °C before use.

PCR primers and a surface primer (Table 2) were selected and designed for the specific detection of *E. coli* based on the *E. coli uidA* gene sequence.[19,20] To support solid-phase PCR, a reverse primer was labelled with Cy3 fluorophores at the 5′ terminal. All of the primers were synthesized and purchased from DNA technology (Aarhus, Denmark).

3.2.2. Immobilization of the surface primer on the top of SAF structure microarrays. 50 μM surface primer with a poly T10C10 tail at the 5′ end was prepared in 5× SSC and 0.004% Triton X, and spotted on the top of SAF structure arrays with the optimal height inside the chamber of a COC chip using the sciLEXARRAYER S5. The polymer chip with the spotted surface primer was then dried at room temperature and treated with UV irradiation at a wavelength of 254 nm with a power of 3 mW cm^{-2} for 10 min (Stratalinker 2400, Stratagene, CA, USA). Under UV irradiation, the poly T10C10-tagged surface primer was stabilized on the plastic surface.[21]

3.2.3. Solid-phase PCR. Before preparing a PCR master mix, each chamber of the chip containing SAF structure arrays with an attached surface primer on top was treated with 2.5 mg mL^{-1} BSA (bovine serum albumin) for 30 min, rinsed with Milli-Q water, dried at room temperature, and then covered with an optical adhesive cover (Applied Biosystems, USA). 25 μL PCR master mix containing 150 nM *uidA* forward primer, 1500 nM *uidA* Cy3-labelled reverse primer, 0.05 U μL^{-1} Phusion Human Specimen DNA polymerase (Thermo Fisher Scientific), and different concentrations of *E. coli* genomic DNA template in 1× Phusion Human Specimen PCR buffer (Thermo Fisher Scientific) was prepared to be loaded into each chamber through the inlet hole. After loading, the inlet and outlet holes were sealed with an optical adhesive cover (Applied Biosystems, USA). The solid-phase PCR was conducted in a ProFlex™ 2× flat PCR system (Thermo Fisher Scientific) at 94 °C for 3 min then followed by 30 cycles at 94 °C for 10 s, 60 °C for 20 s, and 72 °C for 20 s. After the reaction, the chambers were washed 3 times with 4× SSC, 3 times with 0.1× SSC containing 1% Tween-20, and 3 times with deionized water, and dried at room temperature before scanning.

4. Results and discussion

4.1. Chip fabrication and characterization

We designed two different shims (for two batches of experiments), as aforementioned in the chip fabrication in section 2.2. The digital pictures of the two shims and two corresponding chips are shown in Fig. S3 and S4 in the ESI,† respectively. For the details of the micro-milling technique, especially the polishing step so that low surface roughness can be obtained, together with the reproducibility, it is useful to read further in ref. 22.

To observe all the different fabricated heights in one view, we used the chips from batch number 1 for characterisation. Fig. 3a shows the SEM image (side view) of the SAF structures inside one chamber of the polymer chip (fabricated from the first batch). Fig. 3b shows the top view of the SAF structures in the same chamber obtained from the Sensofar optical profiler characterization machine. It is obvious that SAF structures with different heights have been successfully fabricated.

The heights of the SAF structures are shown in Fig. 4. The *y*-axis shows the heights measured using the Dektak XTA stylus profiler. The *x*-axis includes the input heights for the code to run the milling machines. The precision of the milling machines is in the order of ±10 microns due to the

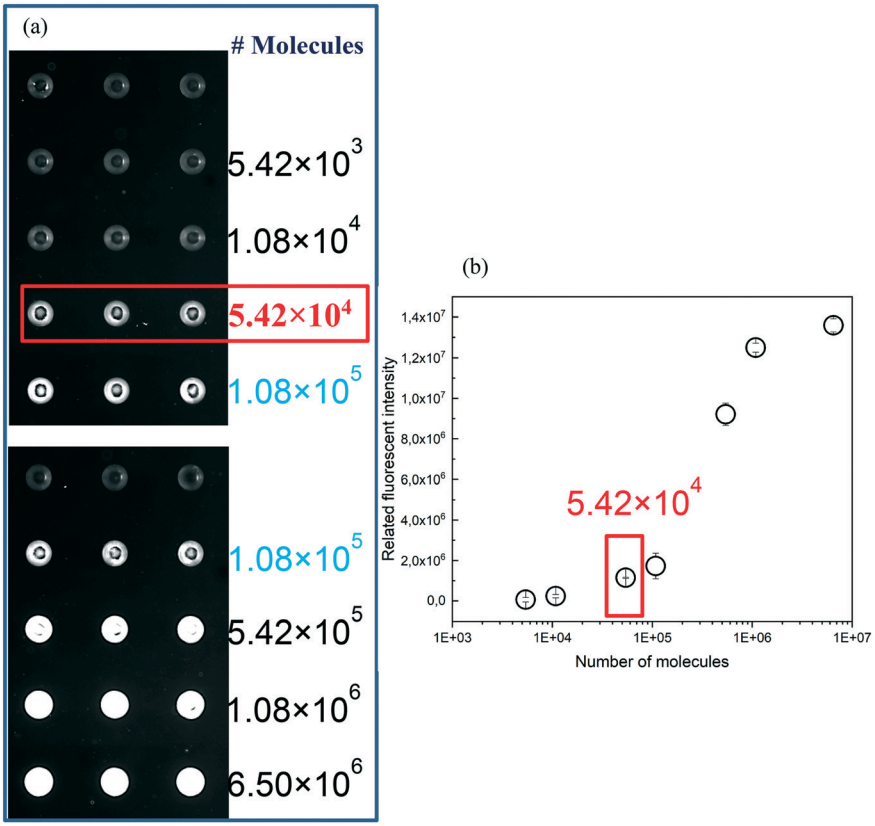

Fig. 8 The LOD of the fluorescence intensity of the optimal SAF structures in the polymer chips. (a) Comparison of the fluorescence scanning images to determine the LOD of the fluorescence intensity. (b) The fluorescence intensity *versus* the number of molecules detected.

surface roughness, the levelling of the milling stage and the limitations of the machine itself.

Fig. 5 shows the SEM images of the top of the milling tool. The diameter of the milling tool measured in the SEM machine is d = 97.4 μm. This number is important since it is used in the modelling to predict the optimal height of the SAF structures (d = 2a, where a is the parameter from our model, see eqn (1)).

4.2. Comparison between experimental and theoretical results from fluorescence spotting on the SAF structures

The experiments were conducted on two batches of chips, as aforementioned in the fabrication section 2.2. In order to compare the fluorescence intensities, chips from batch one are used. In batch number one, each chamber has all the different heights of the SAF structures. It is easier to compare the fluorescence intensities in this case since we can observe all the SAF structures in one chamber under the current field of view of the fluorescence scanner. Chips from batch two, where each chamber has one size of SAF structures, are used in the determination of the detection limit (shown in Fig. 8).

The intensities of Cy3 fluorescence spotted on each SAF structure were analysed using the BioAnalyzer 4F/4S scanner (LaVision Biotec GmbH, Bielefeld, Germany) and are shown in Fig. 6 for the polymer chips in which each chamber contains SAF structures with different heights. The results show that the intensity largely increases linearly with the increase of the SAF height (Fig. 4 and 6) which is maximum when the height is 163 μm which is optimum. Due to the limitations of the milling machine such as its precision in the order of 10 microns, the levelling of the milling table and the hardness of the material, milling down to a large depth dimension (such as in the order of 100 micron depth) is much more precise compared to going down to dimensions near the precision limit (*i.e.* 10 microns near the surface), as shown in Fig. 4. It has been confirmed that the hardness of the material is much more stable and higher when milling down beneath the surface from 100 to 300 microns compared to being milled on the surface with a depth of less than 100 microns.[23]

From eqn (1), by substituting a = 97.4 μm (from Fig. 5), θ = 40.8° and φ = 60°, we obtain the theoretical optimal height of the SAF structures which is equal to 170 μm. The experimental result and theoretical calculation are hence excellently consistent (the limitation of the milling machine with precision in the order of 10 microns). Our method hence opens up opportunities to precisely and massively produce SAF polymer microfluidic chips for use in point-of-care detection. This method can be extended to different kinds of thermoplastic polymers while using different milling tools. As can be seen in eqn (1), the optimal height depends

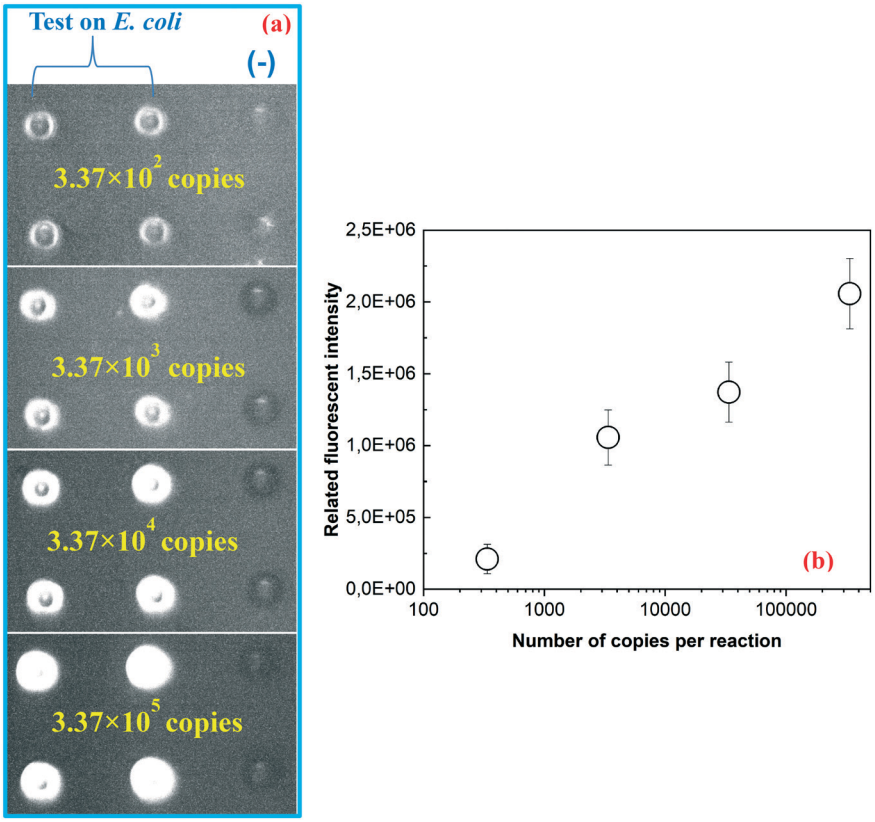

Fig. 9 SP-PCR results on the detection of *E. coli*. (a) Scanning images from the fluorescence scanner. (b) Plot of the fluorescence intensity *versus* the number of *E. coli* genome copies per reaction.

not only on the radius of the milling tip (parameter a) but also on the critical angle (θ), which in turn determines the types of thermoplastic polymers we use. Fig. 7 shows an example of using eqn (1) for the comparison of different fabrication (milling) tools and material conditions in order to produce optimal SAF structures and polymer chips. The brown line in Fig. 7 represents our current experiment in which COC and air are the media we used. As can be seen, once d = 97.4, then a = 48.5 μm, and hence the optimal height of SAF structures is 170 μm. When the measurement is for an aqueous analyte (refractive index n_w = 1.33) and COC, the optimal height is much lower (down to ~40 μm) than that of the air/COC media. Polystyrene (PS, with n_{PS} = 1.59) can also be used in producing polymer chips, and the optimal heights of SAF structures made from PS are shown in red and green lines in Fig. 7.

The polymer chips with the optimal SAF height are then used to determine the fluorescence limit of detection. The results are shown in Fig. 8. Each chamber has 15 SAF structures (Fig. S3a†), and to compare the different molecule concentrations and to determine the limit of detection, the fluorescence intensities are measured in two different chambers on the same chip, as shown in Fig. 8a.

The fluorescence intensity can be described to have a linear relationship with the dye concentration or the number of molecules at a small concentration (dilute solution).[24–26] This relationship is well-known and sometimes called the modified Beer–Lambert relationship,[26] (eqn (S4), ESI†). In Fig. 8, our measurement shows such a relationship. The x-axis of Fig. 8b is plotted in the log 10 scale (to determine the limit of detection). For the linear scale, the result is shown in Fig. S5a in the ESI,† with linear fitting. Fig. S5b† shows the limitation of the linear relationship when the concentration or the number of molecules is high, and this figure has the same form as shown in Fig. 5 of ref. 26.

The fluorescence limit of detection for the current set-up and chips is down to 5.42 × 10^4 molecules (Fig. 8a). In the next section, we use these optimal SAF chips to detect *E. coli* by solid-phase PCR.

4.3. Solid-phase PCR (SP-PCR) to detect *E. coli* using the optimal SAF chips

The optimal SAF chips are used to detect *E. coli* using solid-phase PCR. Fig. 9 shows the results. It is obvious that the optimal SAF chips can successfully and sensitively detect *E. coli* to as low as 3.37 × 10^2 copies (Fig. 9a). Details of fluorescence intensity *versus* number of copies per reaction are shown in Fig. 9b.

5. Conclusion

We present, to the best of our knowledge, for the first time, the theoretical modelling and experimental results on

optimising miniaturised SAF structures in disposable polymer chips used for the highly sensitive detection of pathogens. Our theory is successfully applied and verified by the experimental results on fluorescence intensity measurements for SAF microarrays in COC polymer chips. The method can be extended to any other thermoplastic polymers and micro-milling tools. The results from this work give insights into the fabrication of miniaturised SAF structures used in the rapid and highly sensitive detection of pathogens. This method hence opens up opportunities for the easy mass production of a cheap and efficient biochip for biosensors and point-of-care testing.

Conflicts of interest

There are no conflicts to declare.

Acknowledgements

This research was funded by the European Union's Horizon 2020 research and innovation program, the SMARTDIAGNOS grant agreement No: 687697 and the VIVALDI grant agreement No. 773422.

References

1 J. Enderlein, T. Ruckstuhl and S. Seeger, Highly efficient optical detection of surface-generated fluorescence, *Appl. Opt.*, 1999, **38**(4), 724–732.
2 W. Lukosz and R. E. Kunz, Light emission by magnetic and electric dipoles close to a plane interface. I. Total radiated power, *J. Opt. Soc. Am.*, 1977, **67**(12), 1607–1615, http://www.osapublishing.org/abstract.cfm?URI=josa-67-12-1607.
3 W. Lukosz and R. E. Kunz, Light-Emission by Magnetic and Electric Dipoles Close to a Plane Dielectric Interface .2. Radiation-Patterns of Perpendicular Oriented Dipoles, *J. Opt. Soc. Am.*, 1977, **67**(12), 1615–1619, https://www.osapublishing.org/josa/abstract.cfm?uri=josa-67-12-1615.
4 W. Lukosz, Light-Emission by Magnetic and Electric Dipoles Close to a Plane Dielectric Interface. 3. Radiation-Patterns of Dipoles with Arbitrary Orientation, *J. Opt. Soc. Am.*, 1979, **69**(11), 1495–1503, https://www.osapublishing.org/josa/abstract.cfm?uri=josa-69-11-1495.
5 E. H. Hellen and D. Axelrod, Fluorescence Emission at Dielectric and Metal-Film Interfaces, *J. Opt. Soc. Am. B*, 1987, **4**(3), 337–350, https://www.osapublishing.org/josab/abstract.cfm?uri=josab-4-3-337.
6 D. Axelrod and E. H. Hellen, Emission of Fluorescence at an Interface, *Methods Cell Biol.*, 1989, **30**(C), 399–416.
7 J. Deschamps, M. Mund and J. Ries, 3D superresolution microscopy by supercritical angle detection, *Opt. Express*, 2014, **22**(23), 29081, Available from: https://www.osapublishing.org/oe/abstract.cfm?uri=oe-22-23-29081.
8 T. Q. Hung, Y. Sun, C. E. Poulsen, T. Linh-Quyen, W. H. Chin and D. D. Bang, *et al.* Miniaturization of a micro-optics array for highly sensitive and parallel detection on an injection moulded lab-on-a-chip, *Lab Chip*, 2015, **15**(11), 2445–2451, Available from: http://xlink.rsc.org/?DOI=C5LC00176E.
9 J. Ries, T. Ruckstuhl, D. Verdes and P. Schwille, Supercritical angle fluorescence correlation spectroscopy, *Biophys. J.*, 2008, **94**(1), 221–229, DOI: 10.1529/biophysj.107.115998.
10 D. Hill, B. McDonnell, S. Hearty, L. Basabe-Desmonts, R. Blue and M. Trnavsky, *et al.* Novel disposable biochip platform employing supercritical angle fluorescence for enhanced fluorescence collection, *Biomed. Microdevices*, 2011, **13**(4), 759–767, Available from: https://link.springer.com/content/pdf/10.1007%2Fs10544-011-9546-2.pdf.
11 T. Ruckstuhl, C. M. Winterflood and S. Seeger, Supercritical Angle Fluorescence Immunoassay Platform, *Anal. Chem.*, 2011, **83**(6), 2345–2350, DOI: 10.1021/ac1032758.
12 T. Q. Hung, W. H. Chin, Y. Sun, A. Wolff and D. D. Bang, A novel lab-on-chip platform with integrated solid phase PCR and Supercritical Angle Fluorescence (SAF) microlens array for highly sensitive and multiplexed pathogen detection, *Biosens. Bioelectron.*, 2017, **90**, 217–223.
13 Milling tool DIXI 7006. from http://www.dixipolytool.ch/en/e-shop/?categorie=3&ss_categorie=1&s_coupe=R&no_prod=DIXI%207006 [Internet]. Available from: http://www.dixipolytool.ch/en/e-shop/?categorie=3&ss_categorie=1&s_coupe=R&no_prod=DIXI 7006.
14 J. H. Son, S. Hong, A. J. Haack, L. Gustafson, M. Song and O. Hoxha, *et al.* Rapid Optical Cavity PCR, *Adv. Healthcare Mater.*, 2016, **5**(1), 167–174.
15 J. H. Son, B. Cho, S. Hong, S. H. Lee, O. Hoxha and A. J. Haack, *et al.* Ultrafast photonic PCR, *Light: Sci. Appl.*, 2015, **4**, e280.
16 M. Kemmler, U. Sauer, E. Schleicher, C. Preininger and A. Brandenburg, Biochip point-of-care device for sepsis diagnostics, *Sens. Actuators, B*, 2014, **192**, 205–215.
17 T. Nguyen, S. Z. Andreasen, A. Wolff and D. D. Bang, From Lab on a Chip to Point of Care Devices: The Role of Open Source Microcontrollers, *Micromachines*, 2018, **9**, 403, Available from: http://orbit.dtu.dk/en/publications/from-lab-on-a-chip-to-point-of-care-devices-the-role-of-open-source-microcontrollers(8e205744-3e87-40a1-9d50-2db6af15f6b8).html.
18 T. Q. Hung, W. H. Chin, Y. Sun, A. Wolff and D. D. Bang, A novel lab-on-chip platform with integrated solid phase PCR and Supercritical Angle Fluorescence (SAF) microlens array for highly sensitive and multiplexed pathogen detection, *Biosens. Bioelectron*, 2017, **90**, 217–223, DOI: 10.1016/j.bios.2016.11.028.
19 H. R. M. Schlaman, E. Risseeuw, M. E. I. Franke-van Dijk and P. J. J. Hooykaas, Nucleotide sequence corrections of the uidA open reading frame encoding β-glucuronidase, *Gene*, 1994, **138**(1–2), 259–260.
20 E. Frahm and U. Obst, Application of the fluorogenic probe technique (TaqMan PCR) to the detection of Enterococcus spp. and Escherichia coli in water samples, *J. Microbiol. Methods*, 2003, **52**(1), 123–131.
21 Y. Sun, I. Perch-Nielsen, M. Dufva, D. Sabourin, D. D. Bang and J. Høgberg, *et al.* Direct immobilization of DNA probes

on non-modified plastics by UV irradiation and integration in microfluidic devices for rapid bioassay, *Anal. Bioanal. Chem.*, 2012, **402**(2), 741–748.

22 T. Nguyen, A. Chidambara Vinayaka, D. Duong Bang and A. A. Wolff, Complete Protocol for Rapid and Low-Cost Fabrication of Polymer Microfluidic Chips Containing Three-Dimensional Microstructures Used in Point-of-Care Devices, *Micromachines*, 2019, **10**(9), 624, Available from: https://www.mdpi.com/2072-666X/10/9/624.

23 Z. Pan, Y. Feng and S. Y. Liang, Material microstructure affected machining: A review, *Manuf. Rev.*, 2017, **4**, 5.

24 C. C. Chan, H. Lam and X.-M. Zhang, *Practical approaches to method validation and essential instrument qualification*, Wiley Online Library, 2010, p. 364.

25 D. A. Skoog, F. J. Holler and S. R. Crouch, *Principles of instrumental analysis*, Cengage learning, 7th edn, 2017, p. 368.

26 Joint FAO, *Combined Compendium of Food Additive Specifications*, Analytical methods, test procedures and laboratory solutions used by and referenced in the food additive specifications, 2006, vol. 4, p. 28.